INNOVATIVE MECHANICAL ENGINEERING **ISSN 2812-9229 (Online)**
University of Niš, Faculty of Mechanical Engineering
VOL. 3, NO 2, 2024, PP. 43-55

Original scientific paper*

NUMERICAL SIMULATION OF MHD NANOFLUID FORCED CONVECTION HEAT TRANSFER IN A RECTANGULAR ENCLOSURE WITH VARIABLE PARAMETERS

Ehsan Kianpour[1,2], Seyyed Muhammad Hossein Razavi Dehkordi[1,2], Nor Azwadi Che Sidik[3]

[1]Department of Mechanical Engineering, Najafabad Branch, Islamic Azad University, Najafabad, Iran
[2]Aerospace and Energy Conversion Research Center, Najafabad Branch, Islamic Azad University, Najafabad, Iran
[3]Department of Thermo-fluid, Faculty of Mechanical Engineering, University Technology of Malaysia, Skudai, Johor, Malaysia

Abstract. *This numerical research examines the cooling of a hot obstacle within a rectangular cavity containing water-copper oxide nanofluid. This cavity has an inlet and outlet, and the cold nanofluid comes from the left side of the cavity and goes out from the opposite side, after cooling the hot obstacle. All walls of the cavity are insulated and the SIMPLER algorithm is employed for solving the governing equations. The effect of different parameters such as nanoparticle volume fraction, Reynolds number, and Hartmann number is investigated. The results show that with an increase in the Reynolds number, the isothermal lines become more compact and the dimensions of the cold zone near the inlet increase. This phenomenon causes the isothermal lines to be closer to the hot barrier and the temperature gradient, and as a result the heat transfer of the hot barrier increases.*

Key words: *Cooling, Nanofluid, Numerical simulation, Forced convection, Magnetic field*

1. INTRODUCTION

Since conventional fluids have low thermal conductivity, they limit the rate of heat transfer in industry. Therefore, to increase heat transfer, nanofluids, i.e., dilute

*Received: Avgust 13, 2024 / Accepted October 01, 2024.
Corresponding author: Ehsan Kianpour
Faculty of Engineering, Najafabad branch, Islamic Azad University, Post code: 8514143131
E-mail: (ekianpour@pmc.iaun.ac.ir)

suspensions of nanoparticles in liquids, can be introduced as a practical approach. Many studies have been conducted to extract empirical models for nanofluids and use them in practical examples in nature and industry. In addition, the introduction of some nanofluid applications in cooling systems is a recent and intriguing research topic that has attracted the attention of various researchers [1-5].

Wang et al. [6] numerically investigated the fluid flow and heat transfer of water-copper oxide nanofluid in a square cavity. The horizontal walls were insulated and the left and right walls were hot and cold, respectively. According to their results, when the effect of Brownian motion is taken into account, the average Nusselt number increases with increasing volume fraction. Haddad et al. [7] numerically investigated the effects of Brownian motion in natural convection heat transfer. They conducted a study for water-copper oxide nanofluid in a chamber whose upper and lower walls were cold and hot, respectively. Based on their results, the amount of heat transfer increases in all volume fractions, and of course, this increase effect is more noticeable in low volume fractions. Sharma et al. [8] numerically investigated the forced convection heat transfer of water-alumina nanofluid at low volume fractions in a channel whose walls were heated. According to their results, the average Nusselt number increases in terms of volume fraction of nanoparticles and decreases with the increase in the aspect ratio which was defined as the ratio of width to height. Aghaei et al. [9] considered a trapezoidal enclosure and investigated the velocity field and temperature distribution in such an enclosure using the finite volume method. The working fluid was water accompanied by copper nanoparticles, which led the authors to consider the magnetic field in the enclosure. They found that the nanoparticle volume fraction has a direct effect on increasing the Nusselt number and entropy generation, while the behavior is reversed for the Hartmann number. In another numerical simulation, Abbaszadeh et al. [10] used the KKL model for the CuO-water nanofluid in order to consider the effects of Brownian motions of nanoparticles. The algorithm which they used was SIMPLER with the aim of finite volume method in order to solve the set of Navier-Stokes equations (for obtaining the flow field) and energy equation (for measuring the temperature field). As their problem geometry was a parallel plate microchannel, they considered the slip boundary condition in their walls and the magnetic field effects is reflected in their study by the Hartmann number. They showed that increasing the inertia force of fluid, the nanoparticle density and magnetic field effect increase total entropy production and average Nusselt number. In another study, Ababaei et al. [11] used the FVM numerical method with the goal of finding the optimum location of the impediments to increase the heat transfer rate inside a microchannel. In their study, the working nanofluid was Al_2O_3-water whose characteristics were obtained by Khanafer and Vafaei's [12] model that is a variable properties model. Again, they corroborated the fact that increasing the momentum of the nanofluid will result in the enhancement of the heat transfer inside the microchannel. Therefore, it would be beneficial if we keep the Reynolds number high enough to augment the Nusselt number. For the same reason, the total entropy generation would be increased. Recently, Hashim et al. [13] studied the enhancement of Al_2O_3-water heat transfer inside a wavy cavity using a finite element numerical method. They performed partial heating from the bottom wall while the wavy walls were isothermal and the top wall was insulated. They used different types of oscillations for the wavy walls to find the optimal case in terms of the Nusselt number increase. They showed that nanoparticles

caused an increase in the heat transfer rate inside the cavity. This review of the literature makes it clear that the problem of cooling a hot square-shaped obstacle inside an enclosure has not received significant attention. Therefore, the main objective of the present study is to numerically analyze the cooling of a hot barrier while the magnetic field effects are reflected in the enclosure. The walls of the enclosure are insulated and the effects of fluid inertia, magnetic field strength, volume fraction of nanoparticles and outlet location on the heat transfer rate were investigated. This study was done for Re=1-100, Ha=0-40 and Φ=0-4%.

2. RESEARCH METHODOLOGY

The geometry of the enclosure is shown in Fig. 1. The size of the model of this research is as similar as possible to the dimensions of the models of other research projects [14]. The cold nanofluid (T_c=308K) enters from the left side and after cooling the hot impediment (T_h=372K), it goes out off the opposite site. All of the enclosure walls are insulated and the ratio of the length to width of the enclosure is two. The working nanofluid is MHD CuO-water nanofluid (Table 1). The Navier-Stokes equations accompanied by energy equations for laminar and forced convection of the nanofluid flow are given by:

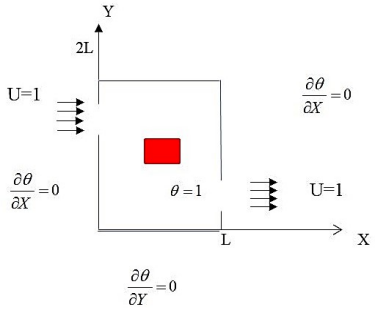

Fig. 1 Geometry and boundary conditions (dimensionless)

Table 1 Thermo-physical properties of water as base fluid and CuO nanoparticles [15]

	ρ (kg/m3)	c_p (J/kgK)	k (W/mK)	d_{up} (nm)	β (K^{-1})	σ (S/m)	μ (Ns/m^2)
pure water	997.1	4179	0.613	--	2.1×10^{-4}	0.05	0.001003
CuO	6500	540	18	29	1.8×10^{-5}	5×10^{7}	--

$$\frac{\partial}{\partial x}\left(\rho_{nf}u\right)+\frac{\partial}{\partial y}\left(\rho_{nf}v\right)=0 \tag{1}$$

$$\frac{\partial}{\partial x}(uu)+\frac{\partial}{\partial y}(vu)=\frac{1}{\rho_{nf}}\left[-\frac{\partial p}{\partial x}+\frac{\partial}{\partial x}\left(\mu_{nf}\frac{\partial u}{\partial x}\right)+\frac{\partial}{\partial y}\left(\mu_{nf}\frac{\partial u}{\partial y}\right)-\sigma_{nf}B_0^2u\right] \tag{2}$$

$$\frac{\partial}{\partial x}(uv)+\frac{\partial}{\partial y}(vv)=-\frac{1}{\rho_{nf}}\frac{\partial p}{\partial y}+\frac{\partial}{\partial x}\left(\nu_{nf}\frac{\partial v}{\partial x}\right)+\frac{\partial}{\partial y}\left(\nu_{nf}\frac{\partial v}{\partial y}\right) \tag{3}$$

$$\frac{\partial}{\partial x}(uT)+\frac{\partial}{\partial y}(vT)=\frac{\partial}{\partial x}\left(\alpha_{nf}\frac{\partial T}{\partial x}\right)+\frac{\partial}{\partial y}\left(\alpha_{nf}\frac{\partial T}{\partial y}\right) \tag{4}$$

In these equations, u and v are the horizontal and vertical components of velocity, p is the pressure, T is the temperature, ρ_{nf} is the nanofluid density, $\nu_{nf}=\mu_{nf}/\rho_{nf}$ is the kinematic viscosity of the nanofluid, $\alpha_{nf}=k_{nf}/\left(\rho c_p\right)_{nf}$ is the thermal diffusion coefficient of the nanofluid, and c_p is the heat capacity of the nanofluid at constant pressure. The dimensionless parameters for casting the mentioned equations into the non-dimensional form are as follows [16]:

$$X=\frac{x}{L},\ Y=\frac{y}{L},\ U=\frac{uL}{\alpha_{bf}},\ V=\frac{vL}{\alpha_{bf}},\ P=\frac{pL^2}{\rho_{nf}\alpha_{bf}^2},\ \theta=\frac{T-T_c}{T_h-T_c},\ \Psi=\frac{\psi}{\alpha_{bf}},\ \Omega=\frac{\omega L^2}{\alpha_{bf}} \tag{5}$$

$$\frac{\partial U}{\partial x}+\frac{\partial V}{\partial y}=0 \tag{6}$$

$$\begin{aligned}&\frac{\partial}{\partial X}(UU)+\frac{\partial}{\partial Y}(VU)=\\&-\frac{\partial P}{\partial X}+\frac{\rho_{bf}}{\rho_{nf}\mu_{bf}}\frac{1}{\mathrm{Re}}\left[\frac{\partial}{\partial X}\left(\mu_{nf}\frac{\partial U}{\partial X}\right)+\frac{\partial}{\partial Y}\left(\mu_{nf}\frac{\partial U}{\partial Y}\right)\right]-\frac{\sigma_{nf}}{\sigma_{bf}}\frac{\rho_{bf}}{\rho_{nf}}\frac{Ha^2}{\mathrm{Re}}U\end{aligned} \tag{7}$$

$$\frac{\partial}{\partial X}(UV)+\frac{\partial}{\partial Y}(VV)=-\frac{\partial P}{\partial Y}+\frac{\rho_{bf}}{\rho_{nf}\mu_{bf}}\frac{1}{\mathrm{Re}}\left[\frac{\partial}{\partial X}\left(\mu_{nf}\frac{\partial V}{\partial X}\right)+\frac{\partial}{\partial Y}\left(\mu_{nf}\frac{\partial V}{\partial Y}\right)\right] \tag{8}$$

$$\frac{\partial}{\partial X}(U\theta)+\frac{\partial}{\partial Y}(V\theta)=\frac{\left(\rho c_p\right)_{bf}}{k_{bf}\left(\rho c_p\right)_{nf}}\times\frac{1}{\mathrm{Re}\,\mathrm{Pr}}\left[\frac{\partial}{\partial X}\left(k_{nf}\frac{\partial\theta}{\partial X}\right)+\frac{\partial}{\partial Y}\left(k_{nf}\frac{\partial\theta}{\partial Y}\right)\right] \tag{9}$$

The Reynolds, Hartmann and Prandtl numbers are defined, respectively, as:

$$\mathrm{Re}=\frac{uL}{\nu_{bf}},\quad Ha=B_0L\sqrt{\frac{\sigma_{bf}}{\mu_{bf}}},\quad \mathrm{Pr}=\frac{\nu_{bf}}{\alpha_{bf}} \tag{10}$$

The properties of the nanofluid including density, heat capacity, volume expansion coefficient, diffusion coefficient are obtained as follows [17]:

$$\rho_{nf}=(1-\varphi)\rho_{bf}+\varphi\rho_s \tag{11}$$

$$\left(\rho c_p\right)_{nf} = (1-\varphi)\left(\rho c_p\right)_{bf} + \varphi\left(\rho c_p\right)_s \tag{12}$$

$$\left(\rho\beta\right)_{nf} = (1-\varphi)\left(\rho\beta\right)_{bf} + \varphi\left(\rho\beta\right)_s \tag{13}$$

$$\alpha_{nf} = k_{nf} \Big/ \left(\rho c_p\right)_{nf} \tag{14}$$

In the Maxwell-Brinkman model, viscosity [13] and thermal conductivity coefficient [15], which are only dependent on the volume fraction of nanoparticles, are obtained from equations (15) and (16).

$$\mu_{nf} = \mu_{bf}\left(1-\varphi\right)^{-2.5} \tag{15}$$

$$k_{nf} = k_{bf}\left[\frac{\left(k_s + 2k_{bf}\right) - 2\varphi\left(k_{bf} - k_s\right)}{\left(k_s + k_{bf}\right) + \varphi\left(k_{bf} - k_s\right)}\right] \tag{16}$$

In the Koo and Kleinstreuer model [18], the viscosity and the coefficient of thermal conductivity are dependent on temperature changes and the effect of Brownian motion. In these models, the viscosity and thermal conductivity coefficient are obtained from equations (17) and (18). The static part of viscosity and the coefficient of thermal conductivity are calculated from equations (15) and (16), and the Brownian part of the coefficient of thermal conductivity and viscosity are obtained from relations (15-18).

$$\mu_{nf} = \mu_{static} + \mu_{Brownian} \tag{17}$$

$$k_{nf} = k_{static} + k_{Brownian} \tag{18}$$

Where $k_{Brownian} = 5\times10^4\,\lambda\varphi\rho_f c_{p,bf}\sqrt{\dfrac{\kappa T}{\rho_s d_p}}\,\zeta\left(T,\varphi\right).\rho_s$

ρ_s and d_p (dp=29×10^{-9}) are the density and radius of nanoparticles, respectively. For the water-copper oxide nanofluid, the λ and ζ functions are experimentally estimated for the range 300<T(K)<325 [3]:

$$\begin{aligned} \lambda &= 0.0137\left(100\varphi\right)^{-0.8229} \quad for \quad \varphi \le 1\% \\ \lambda &= 0.0011\left(100\varphi\right)^{-0.7272} \quad for \quad \varphi > 1\% \end{aligned} \tag{19}$$

κ is the Boltzmann constant. $\left(\kappa = 1.3807\times10^{-23}\ J/K\right)$. $\mu_{Brownian}$ is also obtained from the following equation:

$$\mu_{Brownian} = \frac{k_{Brownian}}{k_{bf}} \times \frac{\mu_{bf}}{\mathrm{Pr}} \tag{20}$$

The local Nusselt number is:

$$Nu = -\frac{k_{nf}}{k_{bf}} \frac{\partial \theta}{\partial n}\bigg|_{wall} \tag{21}$$

where n is the normal direction from the hot obstacle. Thus, the average Nusselt number can be calculated by integrating Eq. (21) along the hot obstacle:

$$Nu_{av} = \frac{\int_L NudL}{\int_L dL} \tag{22}$$

Effective electrical conductivity of the nanofluid was presented by Maxwell [19] as below:

$$\frac{\sigma_{nf}}{\sigma_{bf}} = 1 + \frac{3\left(\frac{\sigma_s}{\sigma_{bf}} - 1\right)\phi}{\left(\frac{\sigma_s}{\sigma_{bf}} + 2\right) - \left(\frac{\sigma_s}{\sigma_{bf}} - 1\right)\phi} \tag{23}$$

The numerical method used in this study is called the SIMPLER algorithm and Finite Volume Method (FVM). In this method, initially, a fine grid should be defined over the problem domain and around each node, and then a volume is considered. Next, after integrating and discretizing equations, the PDEs are simplified. Then, with the help of line-by-line TDMA solver, the discretized equations are solved. In order to choose a suitable network that makes the results independent of the network, the parameters of the average Nusselt number for networks with different dimensions should be compared with each other until the change of the network dimensions does not show much change in those parameters (Table 2).

Table 2 Average Nusselt number in Ha=40, Re=10 and ϕ=0.03

Grid size	Nu_{av}	Relative difference
41×21	19.14	--
81×41	16.10	13.46
161×81	16.38	1.74

3. RESULTS AND DISCUSSIONS

To validate the existing computer program used in this study, the results of Mahmoodi and Sebdani [20] are modeled with the current numerical program and their results are evaluated. The geometry of the Mahmoodi and Sebdani [20] is presented in Fig. 2. They investigated the problem of natural transfer of copper-water nanofluid inside a square enclosure with a square and insulating barrier in the center of the enclosure.

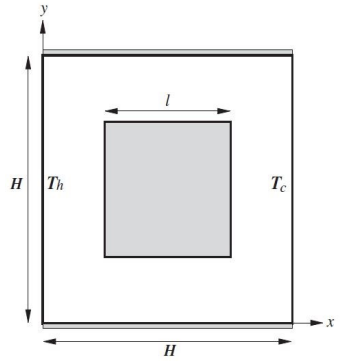

Fig. 2 The geometry of Mahmoodi and Sebdani [20]

As it is clear from Table 3, a good agreement between the results of the present research and the numerical research results of Mahmoudi and Sebdani is present.

Table 3 Comparison of average Nusselt number values on warm wall with Mahmoodi and Sebdani's research [20]

nanoparticle volume fraction	average Nusselt number values		difference percentage
	Mahmoodi and Sebdani	Current study	
ϕ=0.0	9.6762	9.7918	1.2
ϕ=0.05	10.2635	10.4046	1.3
ϕ=0.10	10.8658	10.9789	1.0

Fig. 3 shows the changes of the horizontal component of the dimensionless velocity with respect to the vertical location in the central section of the enclosure at different Reynolds numbers and at Ha=20 and ϕ=4%.

As the Reynolds number increases from 1 to 10, there is little change in the flow pattern because the magnetic forces strongly control the flow (Ha=20). By increasing the Reynolds number to 100, the flow pattern changes to a certain extent in such a way that the suppressive effect of the magnetic field is lost, and in the areas around the speed barrier, it passes the range of 0.3.

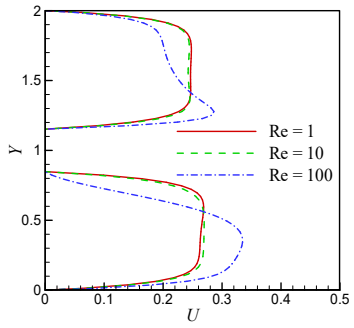

Fig. 3 Variations of the U component velocity with respect to the vertical location in the central section of the enclosure at different Reynolds numbers (Ha=20 and ϕ=4%)

Fig. 4 shows the dimensionless temperature changes with respect to the horizontal and vertical location in the central section of the enclosure at different Reynolds numbers and at ϕ=20% and ϕ=4%. As can be seen from the figure, as the Reynolds number increases, the horizontal and vertical temperature gradient (slope of temperature changes relative to the location) on the hot barrier increases up to four times at X=0.2, X=0.8, Y=0.5 and Y=1.5. Correspondingly, heat transfer will increase as well.

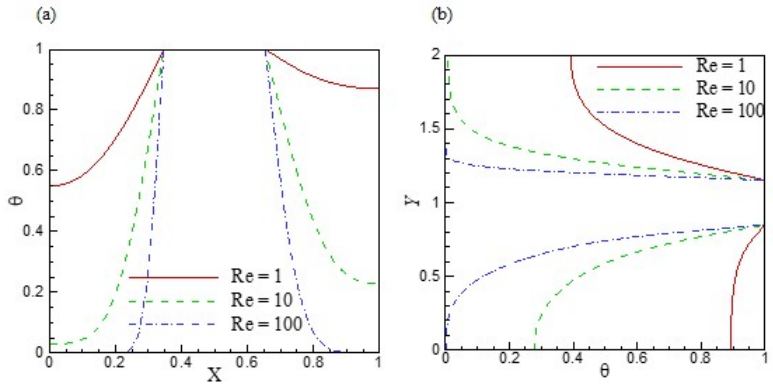

Fig. 4 Dimensionless temperature changes with respect to the (a) vertical location (b) horizontal location in the central section of the enclosure at different Reynolds numbers (Ha=20 and ϕ=4%)

Fig. 5 shows the dimensionless temperature changes with respect to the horizontal and vertical location in the central section of the enclosure at different Hartmann numbers, Re=10 and ϕ=4%. On the left side, the temperature gradient barrier for the case where the Hartmann number is 40 is slightly more than 20 and then zero, because the slope of horizontal temperature changes is greater than in the other cases. This trend is reversed on the right side of the barrier and the temperature gradient for zero. Above the barrier, the

temperature gradient for the case where the Hartmann number is zero is slightly more than 20 and then 40 because the slope of the vertical temperature changes since it is greater than in other cases. The Hartmann number is higher than in the other cases. The reason for this phenomenon is the heating of the fluid under the barrier after passing by it, which reduces the capacity to absorb and transfer heat. It should be noted that in general, the effects of the temperature gradient are more dominant on the left side of the barrier, because in all three Hartmann numbers, a steeper slope is seen there than on the right side of the barrier.

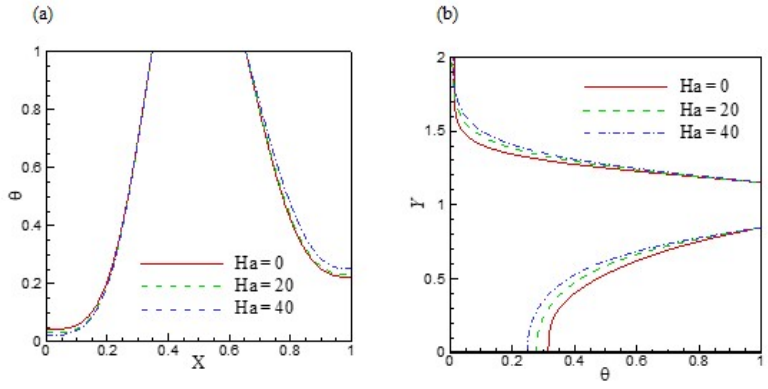

Fig. 5 Dimensionless temperature changes with respect to the (a) vertical location (b) horizontal location in the central section of the enclosure in different Hartmann numbers (Re=10 and ϕ=4%)

Fig. 6 shows the changes of the horizontal component of the dimensionless velocity relative to the vertical location in the central section of the chamber in different Hartmann numbers, Re=10 and ϕ=4%. In general, as the Hartmann number increases from 0 to 40, the current weakens in such a way that in the places where the speed is higher, by applying the magnetic field, the more strongly suppressed current finds a uniform shape by losing its parabolic form. The reason for this phenomenon is magnetic forces, which have a direct but negative relationship with the flow rate $\left(-\left(Ha^2/\mathrm{Re}\right)U\right)$. In this way, at the points where the horizontal speed is higher, the magnetic forces have a stronger weakening effect and the current loses its curved state.

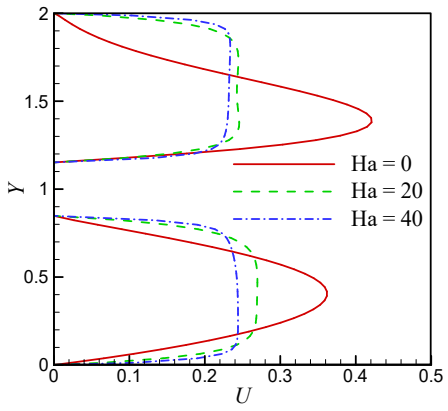

Fig. 6 Variations of the U with respect to the vertical location in the central section of the enclosure in different Hartmann numbers (Re=10 and ϕ=4%)

Fig. 7 shows the changes of the vertical component of the dimensionless velocity with respect to the horizontal location in the central section of the enclosure in different Hartmann numbers and Re=10 and ϕ=4%.

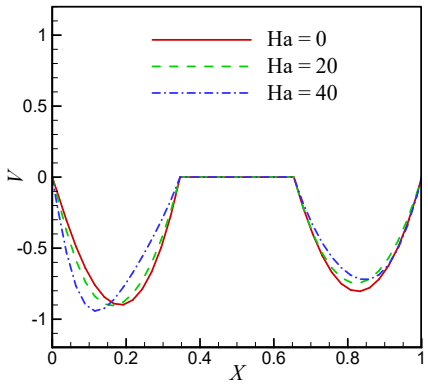

Fig. 7 Variations of the V with respect to the horizontal location in the central section of the chamber in different Hartmann numbers (Re=10 and ϕ=4%)

In general, vertical velocities are lower compared to horizontal velocities. In addition, with the change of the magnetic field, not much change is observed in the pattern of vertical velocities because the magnetic field only affects the horizontal velocities and the term of the dimensionless magnetic force only appears in the horizontal momentum equation.

Fig. 8 shows the dimensionless temperature changes with respect to the horizontal and vertical location in the central section of the enclosure in different nanoparticle volume fractions and Ha=20 and Re=10.

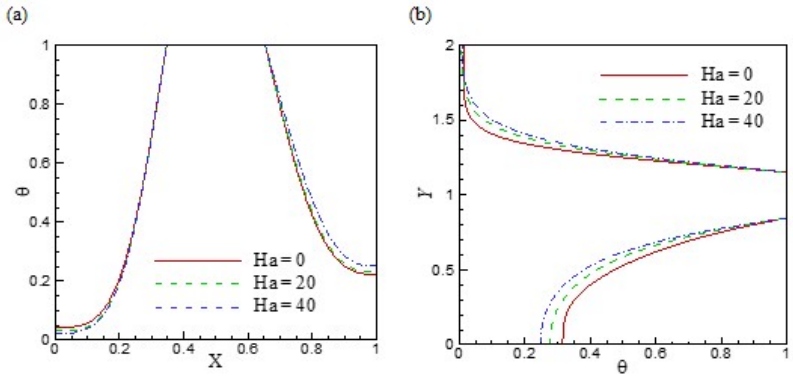

Fig. 8 Dimensionless temperature changes with respect to the (a) vertical location (b) horizontal location in the central section of the enclosure in different nanoparticle volume fractions (Ha=20 and Re=10)

As can be seen from the figure, on the left side, the temperature gradient barrier for the case where ϕ=0% is slightly more than 2% and then 4%, because the slope of the horizontal temperature changes is greater than in the other cases. This process is also maintained on the right side of the barrier. The reason for this is that with the increase in volume fraction, the diffusion coefficient or thermal penetration (α) increases, as a result of which the thickness of the thermal boundary layer increases. Therefore, the temperature gradient will be lower for the nanofluid on the hot barrier. Also, it should be noted that in general the temperature gradient effects are more dominant on the left side of the barrier.

Fig. 9 shows the changes of the U relative to the vertical location and V with respect to the horizontal location within the central section of the enclosure in different nanoparticle volume fractions and Ha=20 and Re=10. By changing the volume fraction of nanoparticles, no change in the flow pattern, vertical velocities and the overall shape of the flow is observed. The reason for this is the insignificant effect of nanoparticles on the viscosity of nanofluid, where the change of the volume fraction of nanoparticles does not affect the viscous properties of the flow, and as a result, its pattern.

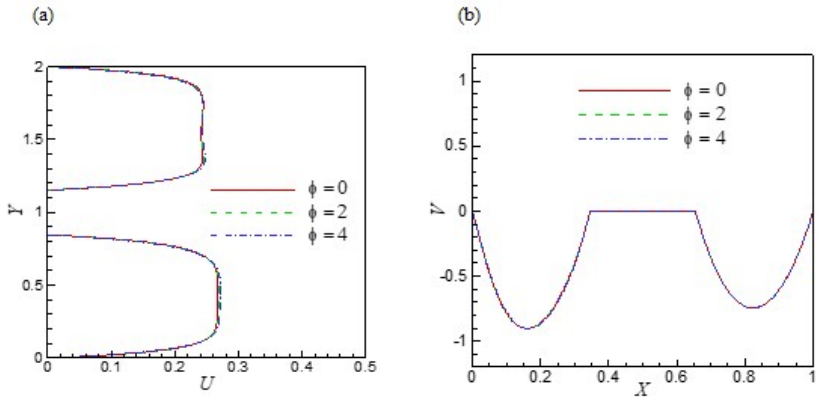

Fig. 8 Variations of the (a) U with respect to the vertical location and (b) V with respect to the horizontal location in the central section of the enclosure in different nanoparticle volume fractions (Ha=20 and Re=10)

4. CONCLUSIONS

In this research, the SIMPLER algorithm and Finite Volume Method were employed to investigate the MHD effects on the flow structure and cooling of a hot barrier in the middle of a rectangular cavity containing water-copper oxide nanofluid. The cavity had an inlet and an outlet, the walls were insulated, the barrier in the middle of the cavity was warm and the effects of fluid inertia, magnetic field strength, and volume fraction of nanoparticles on the heat transfer rate were investigated. The simulation was performed for Re=1-100, Ha=0-40, and ϕ=0-4%. The results showed that:

1. As the Reynolds number increased, the isothermal lines became more compact and the dimensions of the cold zone near the inlet increased. This phenomenon, which is caused by the strengthening of the flow with the increase of the Reynolds number, caused the isothermal lines to be closer to the hot barrier and the temperature gradient, and as a result the heat transfer of the hot barrier increased.
2. By changing the volume fraction of nanoparticles, there was no change in the vertical velocities and the overall shape of the flow. The reason for this issue was the insignificant effect of nanoparticles on the viscosity of nanofluid, where the change of the volume fraction of nanoparticles did not affect the viscous properties of the flow, and as a result, its pattern.

REFERENCES

1. Al-Farhany, K., Abdulkadhim, A., Hamzah, H.K., Ali, F.H., Chamkha, A., 2022, *MHD effects on natural convection in a U-shaped enclosure filled with nanofluid-saturated porous media with two baffles*, Progress in Nuclear Energy, 145, pp. 104136.
2. Alsabery, A.I., Abosinnee, A.S., Al-Hadraawy, S.K., Ismael, M.A., Fteiti, M.A., Hashim, I., Sheremet, M., Ghalambaz, M., Chamkha, A.J., 2023, *Convection heat transfer in enclosures with inner bodies: A review on single and two-phase nanofluid models*, Renewable and Sustainable Energy Reviews, 183, pp. 113424.
3. Giwa, S.O., Sharifpur, M., Ahmadi, M.H., Meyer, J.P., 2021, *A review of magnetic field influence on natural convection heat transfer performance of nanofluids in square cavities*, Journal of Thermal Analysis and Calorimetry, 145, pp. 2581–2623.
4. Mebarek-Oudina, F., Chabani, I., 2022, *Review on Nano-Fluids Applications and Heat Transfer Enhancement Techniques in Different Enclosures*, Journal of Nanofluids, 11(2), pp. 155-168.
5. Rostami, S., Aghakhani, S., Hajatzadeh Pordanjani, A., Afrand, M., Cheraghian, G., Oztop, H.F., Safdari Shadloo, M., 2020, *A review on the control parameters of natural convection in different shaped cavities with and without nanofluid*, Processes, 8(9), pp. 1011.
6. Tongsheng, W., Li, A., Xi, G., Huang, Z. 2023, *Conjugate MHD natural convection of hybrid nanofluids in a square enclosure containing a complex conductive cylinder*, International Journal of Numerical Methods for Heat & Fluid Flow, 33(3), pp. 941-964.
7. Haddad, Z., Iachachene, F., Abu-Nada, E., Pop, I., 2020, *Investigation of the novelty of latent functionally thermal fluids as alternative to nanofluids in natural convective flows*, Scientific Reports, 10(1), pp. 20257.
8. Sharma, M., Sharma, B.K., Kumawat, C., Jalan, A.K., Radwan, N., 2024, *Computational Analysis of MHD Nanofluid Flow Across a Heated Square Cylinder with Heat Transfer and Entropy Generation*, Acta Mechanica et Automatica, 18(3), pp. 536-547.
9. Aghaei, A., Khorasanizadeh, H., Sheikhzadeh, G., Abbaszadeh, M., 2016, *Numerical study of magnetic field on mixed convection and entropy generation of nanofluid in a trapezoidal enclosure*, Journal of Magnetism and Magnetic Materials, 403, pp. 133-145.
10. Abbaszadeh, M., Ababaei, A., Abbasian Arani, A.A., Abbasi Sharifabadi, A., 2017, *MHD forced convection and entropy generation of CuO-water nanofluid in a microchannel considering slip velocity and temperature jump*, Journal of the Brazilian Society of Mechanical Sciences and Engineering, 39, pp. 775-790.
11. Ababaei, A., Abbaszadeh, M., Arefmanesh, A., Chamkha, A.J., 2018, *Numerical simulation of double-diffusive mixed convection and entropy generation in a lid-driven trapezoidal enclosure with a heat source*, Numerical Heat Transfer, Part A: Applications, 73(10), pp. 702-720.
12. Khanafer, K., Vafai, K., 2019, *Applications of nanofluids in porous medium: a critical review*, Journal of Thermal Analysis and Calorimetry, 135, pp. 1479-1492.
13. Hashim, I., Alsabery, A.I., Sheremet, M.A. and Chamkha, A.J., 2019, *Numerical investigation of natural convection of Al2O3-water nanofluid in a wavy cavity with conductive inner block using Buongiorno's two-phase model*, Advanced Powder Technology, 30(2), pp. 399-414.
14. Sheikholeslami, M., Gorji-Bandpy, M., Ganji, D.D. and Soleimani, S., 2014, *Natural convection heat transfer in a cavity with sinusoidal wall filled with CuO–water nanofluid in presence of magnetic field*, Journal of the Taiwan Institute of Chemical Engineers, 45(1), pp. 40-49.
15. Arefmanesh, A., Aghaei, A., Ehteram, H., 2016, *Mixed convection heat transfer in a CuO–water filled trapezoidal enclosure, effects of various constant and variable properties of the nanofluid*, Applied Mathematical Modelling, 40(2), pp. 815-831.
16. Dogonchi, A.S., Selimefendigil, F., Ganji, D.D., 2019, *Magneto-hydrodynamic natural convection of CuO-water nanofluid in complex shaped enclosure considering various nanoparticle shapes*, International Journal of Numerical Methods for Heat & Fluid Flow, 29(5), pp. 1663-1679.
17. Aghaei, A., Sheikhzadeh, G.A., Ehteram, H.R., Hajiahmadi, M., 2015, *MHD natural convection and entropy generation of variable properties nanofluid in a triangular enclosure*, Challenges in Nano and Micro Scale Science and Technology, 3(1), pp. 37-45.
18. Junemoo, K., Kleinstreuer, C., 2004, *A new thermal conductivity model for nanofluids*, Journal of Nanoparticle research, 6, pp. 577-588.
19. Sheikholeslami, M., Gorji-Bandpy, M., Ganji, D.D., Soleimani, S., Seyyedi, S.M., 2012, *Natural convection of nanofluids in an enclosure between a circular and a sinusoidal cylinder in the presence of magnetic field*, International Communications in Heat and Mass Transfer, 39(9), pp. 1435-1443.

20. Mahmoodi, M., Sebdani, S.M., 2012, *Natural convection in a square cavity containing a nanofluid and an adiabatic square block at the center*, Superlattices and Microstructures, 52(2), pp. 261-275.